4−4−20 Anti-Fluorescyl IgG Fab′ Recognition of Membrane Bound Hapten: Direct Evidence for the Role of Protein and Interfacial Structure†

D. E. Leckband,*,‡ T. Kuhl,§ H. K. Wang,|| J. Herron,|| W. Müller,⊥ and H. Ringsdorf⊥

Department of Chemical Engineering, University of Illinois at Urbana−Champaign, Champaign, Illinois 61801, Department of Chemical Engineering, University of California, Santa Barbara, California 93106, Institute for Organic Chemistry, Johannes Gutenburg University, Mainz, Germany, and Department of Pharmaceutics, University of Utah, Salt Lake City, Utah 84112

Received March 20, 1995; Revised Manuscript Received June 27, 1995⊗

ABSTRACT: The surface forces apparatus was used to identify the molecular forces that control the interactions of monoclonal 4−4−20 antifluorescyl IgG Fab′ fragments with fluorescein-presenting supported planar bilayers. At long range, the electrostatic force between oriented Fab′ and fluorescein monolayers was controlled by the composition of the protein exterior surrounding the antigen-combining site rather than by the overall protein charge. The measured positive electrostatic potential of the Fab′ monolayer at pH > $pI_{Fab'}$ was consistent with the structure of the exposed Fab′ surface in which a ring of positive charge at the mouth of the antigen-combining site dominates the local electrostatic surface properties. Substantial differences in the electrostatic forces measured with denatured Fab′ further demonstrated that the measured electrostatic surface properties and the consequent long-range interaction forces are controlled by the protein surface composition. At short range, the strength of the Fab′-mediated adhesion was modulated not only by the length of the fluorescein tether but also by membrane hydration. Steric hydration barriers at the membrane surface reduced the adhesion strength in proportion to their range of influence. These results provide direct evidence that long-range protein interactions with immobilized ligands are controlled by both the protein and the membrane surface compositions, while short-range, specific binding is modulated by both the protein structure and the membrane interfacial properties.

The recognition of membrane-bound receptors is a key event in many critical biological processes such as agonist binding and cell adhesion. In particular, antibody recognition of haptens present on cell surfaces is a key step in eliciting immunogenic responses. Events that involve soluble molecule binding to immobilized receptors can be characterized in terms of (i) the kinetics of surface adsorption and (ii) the binding strength (affinity). The latter events, in contrast to molecular recognition in solution, are further complicated by the influence of the membrane surface composition and structure on receptor−ligand interactions. For example, different cell lines as well as foreign materials exhibit a variety of surface compositions, and surface microenvironments vary widely. Furthermore, membrane structure may also influence receptor presentation and thereby significantly impact the efficacy of soluble ligand binding. Thus, it is of primary concern to determine the molecular basis of both binding kinetics and affinity perturbations by various differences in cell surface or membrane properties.

Site-specific adsorption shares many of the same features as bimolecular recognition events in solution. Namely, in both cases, the binding dynamics are primarily controlled by random Brownian movement at large separations and by directed diffusion governed by molecular and hydrodynamic forces at intermediate-to-short distances from the target molecule or surface (Brune & Kim, 1994; Balgi et al., 1994). On the basis of both Brownian dynamics simulations and coagulation theory, the latter forces are predicted to play a major role in the modulation of bimolecular collision rates (Berg & von Hippel, 1985; Northrup et al., 1987, 1988, 1993; Allison et al., 1985; Allison & McCammon, 1985; Koczak & Subramaniam, 1993). Of the factors that determine the magnitudes and signs of the governing force fields, an increasing body of evidence now suggests that, in addition to the surface or ligand charge, the latter forces are also determined by the composition of the protein exterior (Sharp & Honig, 1990a,b; Northrup et al., 1987, 1988, 1993; Allison et al., 1985; Allison & McCammon, 1985; Koczak & Subramaniam, 1993; Luty et al., 1993). In particular, Brownian dynamics simulations of the association of charged proteins and receptors demonstrated that the charge map of the protein exterior can electrostatically enhance the frequency of productive collisions by guiding the receptors and ligands into their proper binding orientations (Margoliash & Bosshard, 1983; Matthew et al., 1983; Koczack & Subramaniam; 1993; Northrup et al., 1993; Sharp et al., 1987; Luty et al., 1993). On the basis of theoretical models, the composition of the protein exterior outside the binding site clearly influences the rates of bimolecular diffusional encounters. However, the dependence of the noncontact intermolecular forces—forces at intermediate-to-large separations—on the local details of the protein surface composition and, in particular, on the topological variations over the protein surface has only recently been demonstrated by direct measurement (Leckband et al., 1994). Although the latter measurements suggested that the exterior protein

† This work was supported by the National Institutes of Health (PHS GM147334, AI22898, and IR29GM5133801) and by the Whitaker Foundation.

‡ University of Illinois.
§ University of California, Santa Barbara.
|| University of Utah.
⊥ Johannes Gutenberg University.

⊗ Abstract published in *Advance ACS Abstracts,* August 15, 1995.

0006-2960/95/0434-11467$09.00/0

surface may influence bimolecular associations, those findings have not been extended to other systems. Nor have the measured forces been linked to protein function.

In contrast to molecular recognition in solution, at short-range, the local structure and composition of the target surface can substantially impact both the strengths and rates of binding (Leckband et al., 1994; Balgi et al., 1994). In particular, the interface imposes additional steric constraints that are irrelevant in solution reactions. Namely, with small immobilized receptor molecules, long, flexible spacers are required to access the deep binding pockets of the proteins that approach the surface. In addition to the spacer length, the efficacy of receptor presentation also reportedly depends on the spacer mobility, surface density, and solvent compatibility (Ebato et al., 1994; Balakrishnan et al., 1982; Tamm & Bartholdus, 1988; Timbs et al., 1991; McConnell et al., 1986; Ahlers et al., 1992). In many cases, the reported surface binding affinities have been significantly lower than those measured in solution. The latter discrepancies have been attributed to the surface microenvironment (e.g., local pH) (McLaughlin, 1989), to mobility losses (Ebato et al., 1994), to large ligands or receptors—that is, to two-dimensional nonideal excluded area effects (Stankowski, 1983), and to steric hindrance at high receptor surface densities (Tamm & Bartholdus, 1988; Timbs et al., 1991). Although surface electrostatics have been rigorously and extensively investigated (McLaughlin, 1989), the influence of the additional colloidal surface properties, such as surface hydration, have not been considered.

Both the solution and surface binding properties as well as the three-dimensional structures of the monoclonal 4−4−20 antifluorescyl IgG antibody have been extensively characterized (Bedzyk et al., 1990; Krantz et al., 1982; Voss, 1993; Herron et al., 1989, 1994). Consequently, this is an ideal model protein for determinations of the structural factors that influence both the intermolecular forces that control molecular associations and those that influence hapten accessibility in immune recognition. Near diffusion-controlled rates have been reported for the fluorescein−antibody association in solution (Krantz et al., 1982; Voss, 1993). Furthermore, a ring of positive charge surrounds the antigen-combining site. By analogy with other proteins, the rapid solution binding rates may be electrostatically enhanced as the result of the attractive force between the latter positively charged amino acid cluster and the negatively charged fluorescein hapten (Koczak & Subramaniam, 1993; Northrup et al., 1988; Matthews et al., 1983). Despite the latter apparent link between the exterior protein surface composition and protein function, the existence of the requisite electrostatic attractive force—hence, the significance of the local protein structure in hapten−antibody interactions—has not been experimentally verified.

In addition, the 4−4−20 antibody recognition of immobilized fluorescein incorporated in planar bilayers, floating monolayers, and lipid bilayers has been studied by fluorescence microscopy, by ellipsometry, and with a quartz crystal microbalance (Ebato et al., 1992, 1994; Ahlers et al., 1992; Herron et al., 1992). Due to the deep antibody-combining site, spacers of at least 1.5 nm are required for strong antibody binding to the immobilized fluorescein (Ebato et al., 1994). Prior to this work, however, the influence of the membrane interfacial properties on the Fab′ binding efficacy had not been investigated.

In this work, we have used the surface force apparatus (SFA) to directly probe the molecular forces that control the interactions between oriented 4−4−20 antifluorescyl Fab′ fragments and supported bilayer membranes containing fluorescein−lipid conjugates. The forces between the protein and fluorescein monolayers were measured as a function of their separation distance, and the molecular origins of the resultant forces were determined by fitting the experimentally determined force curves to theoretical force profiles. Thus, the electrostatic properties of both the fluorescein and protein monolayers were determined from the measured long-range electrostatic forces between them. The orientational control of the immobilized protein facilitated the direct correlation of the measured forces with a single relative orientation of the interacting molecules, and the dependence of those measured forces on the native protein structure was conclusively demonstrated in measurements with immobilized denatured protein.

The impact of interfacial properties on hapten accessibility and on the consequent Fab′ binding were also examined as a function of the immobilized fluorescein tether length and of the degree of membrane solvation. By determining the dependence of the strength of the Fab′−fluorescein adhesion on both the tether length and the range of steric membrane solvation barriers, we demonstrated that the accessibility of tethered receptors depends not only on the length of the spacer but also on membrane solvation. In particular, the measurement of the steric repulsive forces, their ranges, and their quantitative impact on receptor-mediated adhesion was used to directly probe protein sensitivity to membrane interfacial perturbations.

MATERIALS AND METHODS

Biotinylated 4−4−20 Anti-Fluorescyl IgG Fab′ Fragments. The murine monoclonal antifluorescyl 4−4−20 $IgG_{2a}(\kappa)$ antibody (Mab 4−4−20) was purified from mouse Ascites fluid as described (Ebato et al., 1994). Purified antibodies exhibit an affinity of 5×10^9 M^{-1} at 25 °C (Ebato et al., 1994). The Fab′ fragments were prepared by papain hydrolysis and then biotinylated at a cysteine in the hinge region with *N*-[6-(biotinamido)hexyl]-3′-(2′-pyridyldithio)-propionamide (biotin-HPDP, Pierce) in the presence of a reductant (Ebato et al., 1994). In this work, the biotinylated Fab′ preparation was 75% active, as determined by Scatchard analysis (Ahlers et al., 1992). The protein preparations were homogeneous as determined by polyacrylamide gel electrophoresis and isoelectric focusing. All experiments were completed within 7 days of the Fab′ preparation.

Preparation of Fluorescein and 4−4−20 Anti-Fluorescyl IgG Fab′ Monolayers. 1,1-[(*N*,*N*-Dioctadecylamido)carboxy]-19-(5′-fluoresceinthioureoyl)-4-carboxy-5-oxa-2,8,11,-14,17-pentaoxanonadecane [DODA-$(EO)_4$-FITC] and 1,1-[(*N*,*N*-dioctadecylamido)carboxy]-19-(5′-fluoresceinthioureoyl)-4-carboxy-5-oxa-2,8,11,14,17-trioxanonadecane [DODA-$(EO)_2$-FITC] were synthesized according to published procedures (Ebato et al., 1994). A mixture of 5 mol % DODA-$(EO)_2$-FITC and 95 mol % palmitoyloleoylphosphatidylethanolamine (POPE; Avanti Polar Lipids) was spread at the liquid−vapor interface of a pure water subphase at 25 °C and compressed to a molecular area of 0.70 nm^2/molecule. The fluorescein monolayer was transferred at constant pressure onto a dipalmitoylphosphatidylethanolamine (DPPE; Avanti) monolayer at 0.43 nm^2/molecule

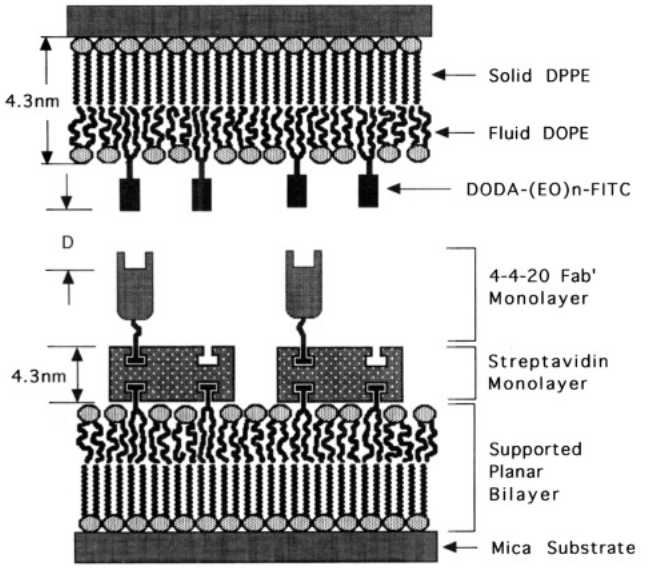

FIGURE 1: Illustration of the oriented, immobilized 4−4−20 antifluorescyl Fab′ monolayer and the opposed membrane bilayer with the fluorescein−lipid conjugate incorporated in the outer leaflet.

supported on a freshly cleaved mica substrate. The resulting supported planar bilayer was then transferred underwater to the apparatus and mounted as described elsewhere (Marra & Israelachvili, 1986). Both the EO_2 and EO_4 forms of DODA-$(EO)_n$-FITC were used in these studies. In some cases, a 2:98 DODA-$(EO)_2$-FITC−POPE mixture was used instead of the 5:95 molar ratio.

Oriented biotinylated Fab′ monolayers were prepared for force measurements by immobilizing singly biotinylated 4−4−20 Fab′ molecules onto homogeneously oriented streptavidin monolayers as follows (Figure 1). First, the streptavidin monolayers were self-assembled onto biotin-presenting planar bilayers supported on mica substrates. Biotinylated supported bilayers were prepared by spreading a monolayer of 5 mol % biotin-X-DPPE (Molecular Probes) in a 95 mol % POPE matrix at the water−vapor interface from a 1:9 methanol−chloroform mixture. The subphase consisted of a 1 mM aqueous NaCl solution at 25 °C. The monolayer was compressed to molecular area of 0.70 nm^2/molecule (Helm et al., 1991; Leckband et al., 1994) and deposited at constant pressure onto a solid DPPE monolayer at 0.43 nm^2/molecule supported on mica. The resulting bilayer was stored in 5 mL of 1 mM phosphate buffer at pH 7.2. To this was added 125 μL of 10^{-6} M streptavidin in 1 M phosphate buffer at pH 7, which had been previously filtered through a 0.1 μm Acrodisc filter (Gelman) and subsequently centrifuged at 5000*g* for 45 min. The streptavidin was incubated with the biotinylated bilayers for 2−3 h at room temperature, after which the treated bilayer was rinsed with 600 mL of 1 M phosphate buffer (pH 7.2) to remove nonspecifically adsorbed streptavidin. The specifically bound streptavidin forms homogeneously oriented monolayers on supported biotinylated lipid bilayers (Häussling et al., 1993; Schmitt et al., 1991). The oriented Fab′ monolayer was then prepared by the addition of 150 μL of 10^{-6} M singly biotinylated 4−4−20 anti-fluorescyl IgG Fab′ to the supported streptavidin monolayer in 5 mL of 1 mM phosphate buffer. Under these conditions, the biotinylated Fab′ forms an oriented monolayer on the streptavidin surface (Ebato et al., 1992; Müller et al., 1993; Herron et al., 1992). Prior to the Fab′ immobilization, the protein solution was filtered and centrifuged as described for the streptavidin solution. A thermally inactivated biotinylated Fab′ preparation was used in control experiments. In all cases, the Fab′ adsorption proceeded for 4 h at room temperature and was followed by a rinse with 750 mL of 1 M phosphate buffer at pH 7.2. The Fab′ sample disk was then transferred underwater to the apparatus and mounted as described (Marra & Israelachvili, 1986).

Force Measurements. Force measurements were conducted with a Mark II surface forces apparatus as described elsewhere (Marra & Israelachvili, 1986). The spectrometer was interfaced with a Dage MTI SIT camera equipped with a Sony 8500 video recorder and video timer.

Two methods were used to obtain the intersurface force vs distance curves. In the first or *dynamic* method, the two opposing surfaces were brought into contact at a constant driving velocity of ∼−2 nm/s (Chan & Horn, 1982). The spring supporting the lower sample deflected under the combined hydrodynamic and colloidal forces, and the static surface forces were determined by subtraction of the hydrodynamic contribution from the total measured force curve. The second or *static* method measured the forces following discreet 2−10 nm decreases in the intersurface separation. In the latter case, the surfaces were brought into contact at an average velocity of ∼−20 nm/min. In some cases, we compared the measurements with both techniques obtained on a given 10 μm^2 contact region of the 1 cm^2 sample surface. Because the rates of intersurface approach differed with the two methods, differences in the resulting force curves would generally indicate the operation of nonequilibrium or time-dependent processes during the interaction (Leckband et al., 1993, 1994).

The force measurements were carried out at 25 °C in 1.0 ± 0.5 mM sodium phosphate buffer (0.5 mM NaH_2PO_4 and 0.5 mM Na_2HPO_4) at pH 7.2 unless specified otherwise. In some cases, the ionic strength was increased by the addition of 10 mL of 1.1 M phosphate buffer (pH 7.2) to the 350 mL of buffer in the chamber housing the samples (final volume ∼360 mL). Halide salts corrode the silver mirrors of the interferometer and cannot be used in these measurements. In all experiments, the solution in the experimental chamber was saturated with POPE to prevent lipid desorption from the bilayers during the measurements.

Theoretical Calculation of DLVO Forces. All measured force profiles were fit to theoretical DLVO force curves—the superposition of electrostatic double layer and the retarded van der Waals forces, including zero frequency screening. The theoretical double-layer force was determined from numerical solutions to the nonlinear Poisson−Boltzmann equation for two interacting charged surfaces in aqueous electrolyte (Chan et al., 1986; Hunter, 1989; Grabbe, 1993). In calculations of the electrostatic double-layer force between two dissimilar surfaces with unequal charge density and sign, both the individual surface potentials and the corresponding electrostatic boundary conditions—such as constant potential or constant charge density—were specified independently for each surface (Chang et al., 1976; Hunter, 1989). Theoretical fits were obtained with software generously provided by A. Grabbe (Grabbe, 1993). In the latter program, the van der Waals force was calculated using the full Lifschitz theory including zero frequency screening by electrolytes (Lifschitz, 1982).

The electrostatic parameters of both surfaces often could not be uniquely determined if both were allowed to vary

freely during the fitting procedure. In this work, however, the charge densities of the DODA-$(EO)_n$-FITC membranes were constrained to values determined from independent measurements of the forces between two identical DODA-$(EO)_n$-FITC membranes (Leckband et al., 1994). The latter sample symmetry simplified the determination of the membrane electrostatic properties and enabled them to be uniquely determined. These values were then used as fixed inputs in the analyses of the Fab′−fluorescein force profiles. Since only the Fab′ electrostatic surface parameters were freely varied, they were uniquely determined in the fitting procedure.

RESULTS

Definition of D = 0 nm. In measurements between identical FITC−membrane bilayers, D = 0 nm referred to the distance between dehydrated lipid head groups on opposing bilayer surfaces. The total thickness of the two bilayers was determined from the measured change in the distance of closest intersurface approach following the drainage of the liquid from the apparatus and removal of the outer lipid monolayers (Marra & Israelachvili, 1985). Based on this procedure, the hydrated thickness of each of the two outer monolayers is half the total thickness change. The theoretical thickness of the outer monolayer Δ_m was calculated from (Leckband et al., 1993; Marra, 1986)

$$\Delta_m = (2V_{hc} + V_{head})/A \quad (1)$$

where V_{hc} is the average hydrocarbon chain volume, V_{head} is the average head group volume, and A is the deposited head group area. With an average ethanolamine head group volume of 0.243 nm^3 (Small, 1967) and a deposited molecular area of 0.70 nm^2, the calculated outer monolayer thickness was 1.6 nm. The thickness of the underlying DPPE monolayer was previously determined to be 2.7 nm (Marra & Israelachvili, 1985); consequently, the total theoretical dehydrated bilayer thickness was 4.3 nm. The measured thickness $2\Delta_m$ of the two hydrated outer membrane monolayers was 10.2 nm. The difference between the theoretical and measured thicknesses—0.8 nm/monolayer—was attributed to adsorbed solvent molecules, to lipid protrusions, and to the finite size of the FITC head group (Israelachvili & Wennerstrom, 1992; LeNeveu et al., 1976; Parsegian et al., 1991; McIntosh et al., 1990; McIntosh & Simon, 1993); consequently, the resulting Stern layer thickness was 0.8 nm in 1 mM phosphate buffer at pH 7.2 and 25 °C.

In force measurements between 4−4−20 Fab′ monolayers and fluoresceinated membrane bilayers, the reference separation (D = 0 nm) was defined as the equilibrium separation between opposed surfaces—that is, the separation at which the surfaces came to rest after spontaneously snapping into adhesive contact under the influence of attractive intersurface forces. The critical force required to detach the adhering Fab′ and FITC surfaces determined the intermembrane adhesive force, or the depth of the attractive minimum (Marra & Israelachvili, 1986; Leckband et al., 1993, 1994, 1995). The distance from which the two surfaces jumped apart under the influence of the applied tensile force was ~1.0 nm farther out from the "equilibrium separation". The difference between the pull-off position and the equilibrium separation was attributed to the extension of the Fab′ and hapten tether under the applied tensile force.

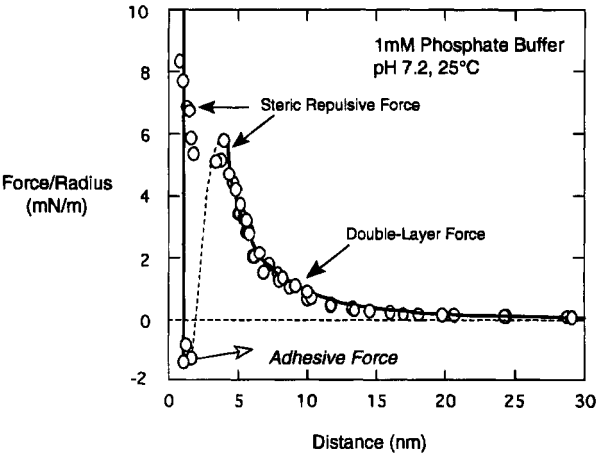

FIGURE 2: Force vs distance curves for the interaction of two 5 mol % DODA-$(EO)_2$-FITC−95% POPE planar bilayers in 1 mM phosphate at pH 7.2 and 25 °C. At $D > 4.8 \pm 0.2$ nm, the force curves (open circles, N = 3) are well-described by DLVO theory (solid line) with the best fit surface charge density of −6 mC/m^2 and the experimentally determined Debye length of 4.3 nm. The outer Helmholtz plane was set at 4.8 nm, and the van der Waals plane of origin was assumed to lie at D = 0 nm. At $D < 4.8$ nm, the soft steric repulsion was attributed to the repulsive interactions between the fluorescein head groups. The steric repulsive force collapsed as the head groups interdigitated, and the surfaces jumped into an adhesive minimum at $D = 1.5 \pm 3$ nm. The depth of the minimum was determined by the force necessary to pull the surfaces apart, as indicated by the outward-directed arrow.

The Fab′ monolayer thickness of 4.2 nm was also determined from the change in the distance of closest intersurface approach following the destruction of the entire sample by ultraviolet irradiation (Hg−Ar pen ray) for 8 h at 25 °C under a stream of filtered nitrogen. The total thickness change was equal to the sum of the thicknesses of the two bilayers plus those of the streptavidin and Fab′ monolayers (Figure 1). The hydrated fluorescein− and biotin−lipid monolayers and the streptavidin monolayer thicknesses were 5.1, 4.3, and 4.3 ± 0.2 nm, respectively (Marra & Israelachvili, 1985; Helm et al., 1991; Leckband et al., 1992, 1994); consequently, the Fab′ monolayer thickness was determined from

$$T(\text{Fab}') = \Delta - [(5.1 + 4.3\ \text{nm}) + 4.3\ \text{nm}] \quad (2)$$

where T is the Fab′ layer thickness and Δ is the total sample thickness change following sample destruction. The thickness change Δ of 17.9 ± 0.3 nm corresponded to a Fab′ thickness of 4.2 ± 0.3 nm and was consistent with the crystallographically determined Fab′ thickness, if the protein normal was oriented to expose the binding site to the opposed membrane (Ebato et al., 1992). This was confirmed by analysis of the crystallographically determined structure with the coordinates supplied by Herron and BIOSYM molecular graphics software. An earlier study reported a 7 nm Fab′ monolayer thickness (Herron et al., 1992), but in that work, the Fab′ was multiply biotinylated via amine groups, and its immobilized orientation was not well-defined as in this study. Moreover, the previous measurements determined the optical Fab′ thickness based on an assumed protein index of refraction, whereas these force measurements directly report the steric thickness of the protein layer.

Molecular Forces between DODA-$(EO)_n$-FITC Bilayer Membranes. Figure 2 shows the resulting force curve for the interaction between two identical 5 mol % DODA-$(EO)_2$-FITC monolayers in 1 mM sodium phosphate buffer at pH

7.2. $D = 0$ nm refers to dehydrated bilayer contact. The force profile at $D > 4.8 \pm 0.5$ nm was described by the DLVO theory of electrostatic double layer plus van der Waals forces (Hunter, 1989; Israelachvili, 1992). The experimentally determined 3.4 nm Debye length was close to the theoretical value of 4.3 nm calculated from (Israelachvili, 1992)

$$\lambda_D = \kappa^{-1} = \left(\frac{\sum_i c_i e^2 z_i^2}{\epsilon \epsilon_0 kT} \right)^{-1/2} \quad (3)$$

where c_i is the bulk concentration of the ith species, z_i is its charge, e is the electronic charge, ϵ is the medium permittivity, ϵ_0 is permittivity of free space, k is the Boltzmann constant, and T is the absolute temperature.

At $D \approx 4.8$ nm, however, the measured curve deviated from theory, and a steep steric repulsive force was measured. The non-DLVO steric force eventually collapsed, however, and the surfaces jumped into an adhesive minimum at $D = 1.5 \pm 0.2$ nm. The range of the soft steric repulsion (4.8 nm) was consistent with the ~2 nm dimension of the fluorescein head group plus the poly(ethylene oxide) (PEO) spacer—~2 nm/surface (Ahlers et al., 1992); consequently, the repulsive force at 4.8 nm was attributed to steric interactions between the fluorescein head groups (Leckband et al., 1992, 1994). Due to the mobility conferred by the long tether and to the large lateral inter-fluorescein spacing, the head groups could easily reorient to alleviate the electrostatic and steric repulsion between them. The subsequent collapse of the repulsive force and the jump into adhesive contact at $D = 1.5 \pm 0.2$ nm accompanied the reorientation and interdigitation of the extended head groups. The depth of the minimum at the latter equilibrium separation was determined from the tensile force required to separate the surfaces, the adhesion force, and was $F_{adh}/R = -0.8 \pm 0.3$ mN/m. At smaller separations ($D < 1.5$ nm), the intersurface repulsion increased sharply since the hard steric repulsion between hydrated lipid head groups prevented closer approach.

The electrostatic surface parameters and the Hamaker constant that gave rise to the charged bilayer interactions were obtained from fits to the data at D at $> 4.8 \pm 0.2$ nm to theoretical DLVO force curves. The best fit parameters were obtained with the *constant surface charge* boundary condition (Chan et al., 1976; Hunter, 1989), the outer Helmholtz plane or the plane of charge set at $D = 4.8$ nm, and the van der Waals plane of origin set at $D = 0$ nm. The estimated location of the plane of charge was consistent with the position of the negatively charged fluorescein head groups, ~2 nm from each surface.

The best fit surface potential and surface charge density were -51 ± 3 mV and -6 ± 1 mC/m^2, respectively. This corresponded to 27 nm^2/charge, or a head group ionization of 14/27 = 0.55. This was lower than expected based on the hydroxyl and free carboxy pK's (Kibblewaite et al., 1989; Martin & Linqvist; 1975; Omelyanenko et al., 1993). Reported low degrees of ionization of charged monolayers have been attributed to the energy cost of charging the surfaces (Helm et al., 1986; Leckband et al., 1993). Moreover, in these fits, we assumed that all charged head groups were ~4.8 nm from the lipid surface. Since the spacers are somewhat flexible, the latter assumption most likely overestimated the true location of the outer Helmholtz plane. This would result in an underestimation of the surface charge density and the degree of ionization (Marra, 1986). The fitted Hamaker constant was 7×10^{-21} J, which was reasonable, if the van der Waals plane of origin lay near the lipid head groups rather than at the plane of the sparse hydrophilic fluorescein moieties.

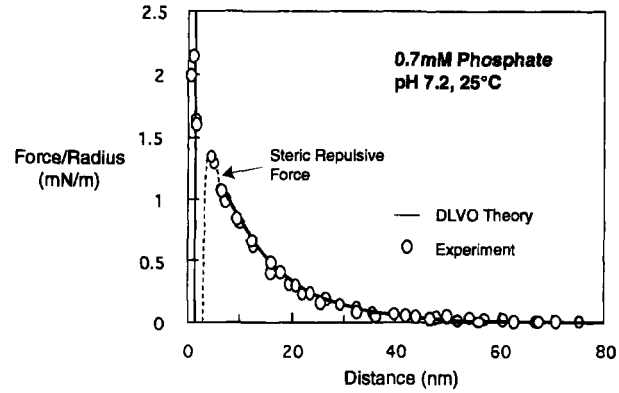

FIGURE 3: Force vs distance curves for the interaction of 2 mol % DODA-$(EO)_2$-FITC−95% POPE planar bilayers in 0.7 mM phosphate at pH 7.2 and 25 °C. The force curves (open circles, $N = 2$) are described by DLVO theory (solid line) with the best fit parameters given in the text.

The Hamaker constant was also estimated from the magnitude of the total attractive force—the difference between the total repulsive force and the adhesive force at the position of the minimum (Leckband et al., 1993). If the intersurface attraction is due only to the van der Waals force, then the Hamaker constant can be determined from the total attractive force at the minimum and (Israelachvili, 1992)

$$A \approx 6F_{attr}\Delta D^2/R \quad (4)$$

where ΔD is the distance from the van der Waals plane of origin (taken as $D = 0$ nm). Thus, the Hamaker constant of 1.1×10^{-20} J was determined with the estimated attractive force of 4.8 + 0.8 = 5.5 mN/m (Figure 2), $\Delta D = 1.5$ nm, and eq 4. The significant deviation from the fitted value may be attributed in part to the action of additional attractive forces between the membranes such as hydrophobic interactions, hydrogen bonding, or aromatic stacking interactions between the fluorescein head groups (Marra & Israelachvili, 1985; Leckband et al., 1993). Additionally, the positions of the van der Waals plane and the outer Helmholtz plane differ for these surfaces. This likely resulted in some error in the estimate of the repulsive electrostatic contribution at $D = 1.5$ nm. Moreover, the uncertainty in the exact location of the van der Waals plane may also result in errors in the calculated Hamaker constant (Marra & Israelachvili, 1985, 1986). Due to these uncertainties, the fitted Hamaker constant was considered the more reliable value.

Forces measured between 2 mol % fluorescein surfaces at 35.0 nm^2/fluorescein (Figure 3) differed from the observed interactions between 5 mol % fluorescein bilayers. At $D >$ 5 nm, the force profile was also described by DLVO theory, but the non-DLVO steric force at 4.8 nm was not as prominent. This behavior was consistent with the observed differences between 5 and 0.5 mol % biotin−lipid containing bilayers (Leckband et al., 1994). With the 2 mol % fluorescein membranes, the surfaces jumped into adhesive contact from a separation distance of 5.5 nm (Figure 3), and only a small deviation from the theory suggested any fluorescein head group overlap. The depth of the minimum

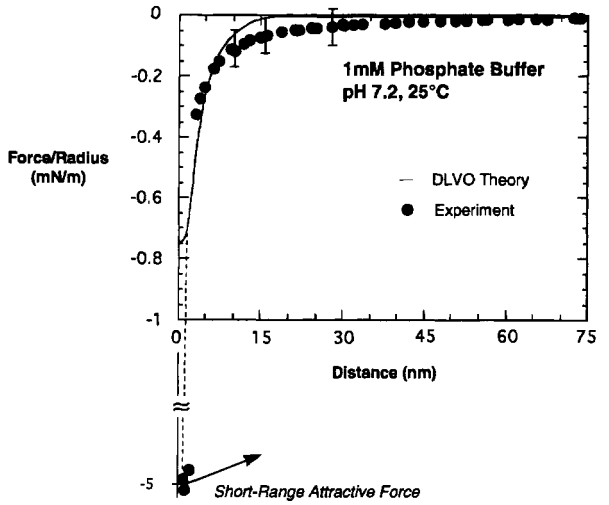

FIGURE 4: Force vs distance profile for the interaction between an oriented 4−4−20 Fab′ monolayer and a 5 mol % DODA-$(EO)_2$-FITC membrane bilayer in 1 mM phosphate buffer at pH 7.2 and 25 °C. The solid line through the experimental data (open circles, $N = 2$) represents the best fit to the DLVO theory with a constant FITC membrane charge of −6 mC/m^2, a Fab′ monolayer electrostatic surface potential of 5 ± 2 mV, and the experimentally determined Debye length of 3.4 nm.

was −1.7 ± 0.1 mN/m, and corresponded to $A = (2 \pm 1) \times 10^{-20}$ J. The greater short-range adhesion was most likely due to a reduced short-range steric repulsion as the result of fewer fluorescein head groups in the gap. From fits of the force data for the 2% DODA-$(EO)_2$-FITC monolayer interactions in 1 mM phosphate buffer at pH 7.2 and 25 °C to the theoretical DLVO force curve, the constant surface potential was −50 ± 5 mV or −4.7 mC/m^2. As with the 5 mol % fluorescein−lipid membranes, the outer Helmholtz plane was assumed to lie at 4.8 nm since the head groups were likely extended at both coverages. At 35 nm^2/FITC head group, the fitted charge density corresponded to 35 nm^2 per FITC/34 nm^2 per charge, or 100% ionization.

Forces between 4−4−20 IgG Fab′ and 5% DODA-$(EO)_2$-FITC Bilayers. The force vs distance profile for the interaction between monolayers of 4−4−20 IgG Fab′ and a 5 mol % DODA-$(EO)_2$-FITC bilayer was determined at pH 7.2 in 1 mM phosphate at 25 °C (Figure 4). Figure 4 shows the initial interaction forces, measured by the *dynamic method*, between two previously unperturbed surface layers. At pH 7.2, the solution pH exceeded the Fab′ isoelectric point (pI = 6.8), and the protein charge was net negative. Because the pH also exceeded the pK's of 6.4 and 4.4 for the fluorescein hydroxyl and carboxylic acid groups, respectively (Omelyanenko et al., 1993; Martin & Linqvist, 1975), the membrane surface charge was also presumed to be negative. Despite the latter considerations, the measured force curve was attractive at D < 30 nm. The magnitude of the short-range adhesive force between the fluorescein and Fab′ monolayers at D = 0 nm was −5.0 ± 0.1 mN/m, as determined by the force required to detach the surfaces.

The force curves measured by the dynamic method were identical with those determined by static method. This demonstrated that the results were independent of the data acquisition method used. Consequently, the independence of the forces on the compression rate demonstrated the absence of nonequilibrium or time-dependent events during the interactions and ensured that both techniques measured the equilibrium forces (Leckband et al., 1994). However, after successive (>2 − 3) contacts, the depth of the short-range minimum decreased, and the long-range forces became more repulsive, or less attractive. This behavior was similar to previous observations where surface detachment damaged the two surfaces by the pull-out of lipid anchors (Leckband et al., 1994, 1995). It is also likely that in this case repeated compression cycles may have also denatured the proteins. Since the initial strength of adhesion did not recover over a period of >4 h, the treatment was assumed to have irreversibly damaged the sample surfaces in the contact region.

Table 1: Electrostatic Surface Potentials of Oriented 4−4−20 FAB′ Monolayers

protein	spacer	FITC density (nm^2/FITC)	buffer concn (mM)	Fab′ potential[a] (mV)[a]
active 4−4−20	EO2	14	1	5 ± 2
active 4−4−20	EO2	14	30	5 ± 2
active 4−4−20	EO2	35	1	−3 ± 3
active 4−4−20	EO4	14	1	7 ± 2
inactive 4−4−20	EO2	14	0.3	−55 ± 5[b]

[a] Constant potential. [b] Constant charge density.

The electrostatic origin of the Fab′−5 mol % fluorescein forces was established on the basis of data fits to theoretical DLVO force profiles. In the latter fits, the electrostatic parameters of the fluorescein bilayer surfaces were constrained by the bounds of the previously determined *constant surface charge density* of −6 ± 1 mC/m^2 (−51 mV), and only the electrostatic properties of the Fab′ monolayer were freely varied. In all cases, the plane of charge was set at the equilibrium membrane−Fab′ separation distance, D = 0 nm. The charges are topologically distributed over the rough Fab′ surface, but in these measurements, we determined the average electrostatic potential at the plane tangent to the protein surface, which determined the distance of closest approach of the opposed surfaces. The best fit to the data was obtained with a constant Fab′ electrostatic surface potential of +5 ± 2 mV (Table 1) and a Hamaker constant of 10^{-21} J. The low fitted Hamaker constant was attributed to the small area of molecular contact between the Fab′ and opposed bilayer surface due to the low Fab′ surface coverage and to the protein's intrinsic roughness. With a Fab′−streptavidin stoichiometry of 1:1 (Herron et al., 1992; Ebato et al., 1994), and a streptavidin surface coverage of 45.0 ± 0.5 nm^2/streptavidin (Vaknin et al., 1993; Schmitt & Knoll, 1991), the calculated Fab′ charge based on these measurements was 0.2 unit charge/Fab′. Despite the overall negative Fab′ charge, the negative fluorescein membrane electrostatic potential ensured that the measured electrostatic surface potential of the Fab′ monolayer was unambiguously positive (Leckband et al., 1994). In these measurements, however, the oriented Fab′ presented the positively charged surface surrounding the antigen-combining site to the opposed membrane. Consequently, these results suggested that the local details of the interacting protein surface, not the overall protein charge, determined the resultant long-range forces.

The electrostatic origin of the long-range Fab′−fluorescein attractive force was verified in measurements at increased ionic strength. For the data shown in Figure 5, the total phosphate buffer concentration was increased to 30 mM. As expected, the range and magnitude of the long-range attractive force decreased significantly. Surprisingly, the short-range adhesion also decreased from −5.0 to −3.0 ± 0.5

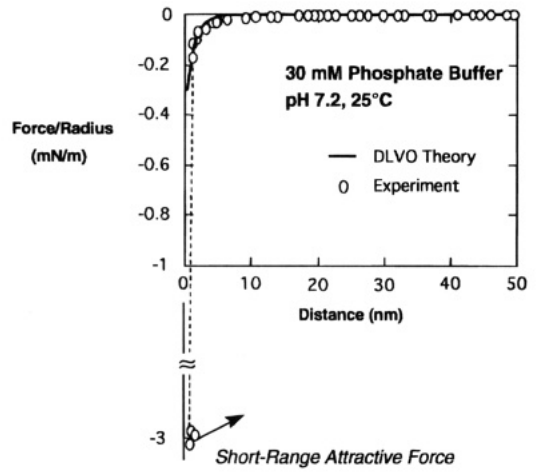

FIGURE 5: Force vs distance profile for the interaction between an oriented 4−4−20 Fab′ monolayer and a 5 mol % DODA-$(EO)_2$-FITC membrane bilayer in 30 mM phosphate buffer at pH 7.2 and 25 °C. The solid line through the experimental data (open circles, $N = 2$) represents the best fit to the DLVO theory. The curve was calculated with the constant FITC membrane charge of −6 mC/m^2, a Fab′ monolayer electrostatic surface potential of 5 ± 2 mV, and the experimentally determined Debye length of 1.1 ± 0.5 nm.

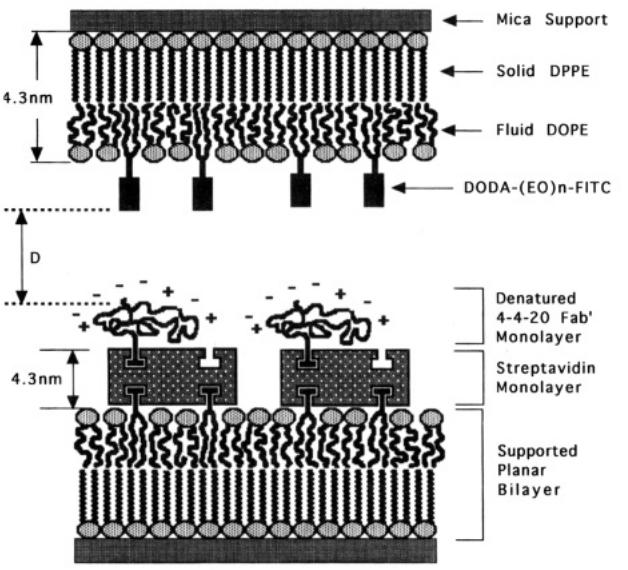

FIGURE 6: Illustration of the interaction between denatured, immobilized 4−4−20 Fab′ monolayers and a planar 5 mol % DODA-$(EO)_2$-FITC lipid bilayer.

mN/m. The changes in the intermediate- to long-range forces, however, were consistent with expectations based on the low ionic strength data (Figure 4), namely, the best fit parameters for the fluorescein and Fab′ surfaces were −6 ± 1 mC/m^2 and +5 ± 1 mV (Table 1), respectively, in complete agreement with the values determined in 1 mM buffer. Again, the fitted Hamaker constant was 10^{-21} J. The good agreement between the fitted surface parameters at both ionic strengths demonstrated that the long-range forces were electrostatically controlled and that the ionic strength-dependent force attenuation was not due to salt-induced protein structural perturbations. Moreover, the agreement between the Fab′ electrostatic surface potentials obtained at the different ionic strengths demonstrated that the underlying streptavidin monolayer did not influence the measured Fab′ electrostatic surface properties. This was consistent with the low electrostatic surface potential of streptavidin at pH 7.2 and with the Fab′ dimensions (4.2 nm) relative to the measured Debye length of 3.4 nm (Leckband et al., 1994; Helm et al., 1991).

The strength of the specific Fab′−fluorescein adhesion was determined from the deviation of the force curve from DLVO theory at $D = 0$ nm. This approach was used to determine the adhesive strength of specific streptavidin-mediated cross-bridges between biotinylated membranes (Leckband et al., 1994). Both nonspecific DLVO forces and the specific short-range adhesive force determined the depth of the attractive minimum (*cf.* Figure 2). In these force measurements, the receptor-mediated cross-bridges were assumed to rupture via lipid distraction, such that the "specific adhesion" reflected the cross-bridge density in the contact region but not the receptor−ligand bond energies (Leckband et al., 1995; Evans et al., 1992; Bell, 1978). Consequently, changes in the specific adhesive force would reflect changes in the bond formation probability—due to, for example, the presence of steric energy barriers—rather than in the intrinsic bond energy. The interactions that determine the lipid distraction force are independent of the DLVO forces, and the assumed additive contribution of the DLVO and lipid pull-out forces to the short-range attractive force is justified. Thus, by subtracting the DLVO contribution from the short-range attractive force, we determined the specific adhesive forces measured with the 1.8 nm spacer to be −4.3 and −2.7 mN/m in 1 and in 30 mM phosphate buffer, respectively.

The expected Fab′−membrane adhesive strength was estimated on the basis of (1) previously measured lipid distraction forces, (2) a Fab′ surface coverage of 45.0 ± 0.5 nm^2/molecule, (3) the measured 75% Fab′ activity, and (4) the apparent absence of fluorescein photobleaching. At ∼23 nm^2/cross-bridge, the measured streptavidin−biotin-lipid distraction force was −32 ± 4 mN/m, and the expected Fab′−fluorescein membrane adhesive force was therefore −32 mN/m × (1 Fab′ site/2 streptavidin sites)(0.75 active Fab′/total immobilized Fab′) = −12 mN/m. Clearly, the specific adhesion measured with the 1.8 nm DOCA-$(EO)_2$-FITC spacer was significantly lower than anticipated at both buffer concentrations.

Force Measurements with Thermally Denatured Fab′. The measured electrostatic surface properties of the Fab′ monolayers suggested that the local details of the exposed protein surface determined the forces that govern the long-range Fab′−hapten interactions. This hypothesis was verified in measurements with thermally denatured Fab′. Denaturation randomized the protein structure, and the resulting protein surface layer presumably exhibited an average surface charge similar to the net negative charge of the Fab′ (Figure 6). This was in sharp contrast to the previous case, where >75% of the immobilized Fab′ exposed a single folded surface to the hapten-presenting membrane.

As shown in Figure 7, the resulting force profile, measured at pH 7.2 and 25 °C, was repulsive at separations less than 50 nm, and there was no short-range specific attraction. In these measurements, $D = 0$ nm was defined by the position of steric contact between the outer Fab′ surface and the fluorescein−membrane. The electrostatic potential of the denatured Fab′ monolayer was determined as described for the native protein measurements. In the fits, both the Fab′ electrostatic surface potential and the charge regulation boundary condition were varied. The best fit was obtained with the *constant charge density* boundary condition for both the fluorescein and the Fab′ monolayers and the corresponding fitted charge densities of −7.0 ± 0.5 and −7.5 ± 0.5 mC/m^2 (−55 mV), respectively, at pH 7.2 in 0.3 mM

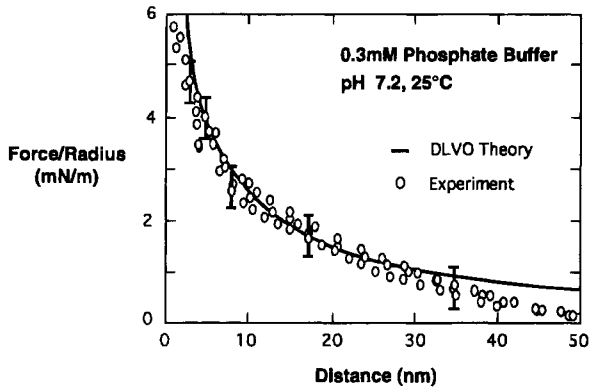

FIGURE 7: Force vs distance profile for the interaction between denatured 4−4−20 Fab′ and a 5 mol % DODA-$(EO)_2$-FITC membrane bilayer in 0.3 mM phosphate buffer at pH 7.2 and 25 °C. The solid line through the experimental data (open circles, $N = 4$) is the best fit to DLVO theory, calculated with the constant FITC membrane and Fab′ monolayer surface charge densities of -7 ± 1 and -7.5 ± 1 mC/m^2, respectively, and the experimentally determined Debye length of 10.1 nm.

phosphate buffer (Table 1). The latter value corresponded to 21.3 nm^2/charge—that is, a net charge of −2.3/Fab′. In marked contrast to the active Fab′ monolayer, the inactive Fab′ surface charge was net negative, and the surface charge—not the potential—was constant at all separations. The latter alteration of the electrostatic boundary condition was similar to previous observations that the carboxyls of bound biotins altered the boundary conditions controlling streptavidin electrostatic interactions (Leckband et al., 1994). Consequently, these results demonstrate that the protein surface composition not only controls the electrostatic surface potentials but also regulates the electrostatic surface potential as a function of the intermolecular separation.

Effect of FITC Coverage. At high ligand surface densities, the excluded ligand area can sterically impede protein binding to the immobilized molecules (Tamm & Bartholdus, 1988; Spinke, 1993). The possibility that high fluorescein surface densities may have reduced the specific Fab′−fluorescein adhesion was tested by reducing the FITC surface density from 5 to 2 mol %. Under these conditions, the area per FITC was increased from 14 to 35 nm^2/head group, compared with the 0.70 nm^2/lipid and ~45 nm^2/Fab′. Thus, the Fab′:fluorescein ratio was reduced from 1:4 to 1:1.6 upon reduction of the fluorescein−lipid surface concentration. Although the double-layer force was expected to decrease in response to the reduced fluorescein−membrane surface charge, since the Fab′ coverage was still limiting (Fab′/FITC < 1), the number of Fab′−fluorescein cross-bridges, hence the specific adhesion, was not expected to change significantly in the absence of steric impediments.

As expected, the measured force curves were similar to those measured with 5 mol % fluorescein, but the long-range electrostatic force was less attractive and the force curve was repulsive at short range (Figure 8). The short-range adhesive force, including both nonspecific and specific contributions, was -5.3 ± 0.3 mN/m. The best fit of the long-range force was obtained with -45 ± 3 (-3.8 mC/m^2) and -3 ± 3 mV for the FITC membrane and Fab′ monolayer surface potentials, respectively, and with a Hamaker constant of 10^{-21} J (Table 1). The deviation from theory at $D < 2$ nm was attributed to nonequilibrium steric or hydrodynamic forces. Similar short-range repulsive forces have been observed in dynamic measurements and attributed to time-dependent

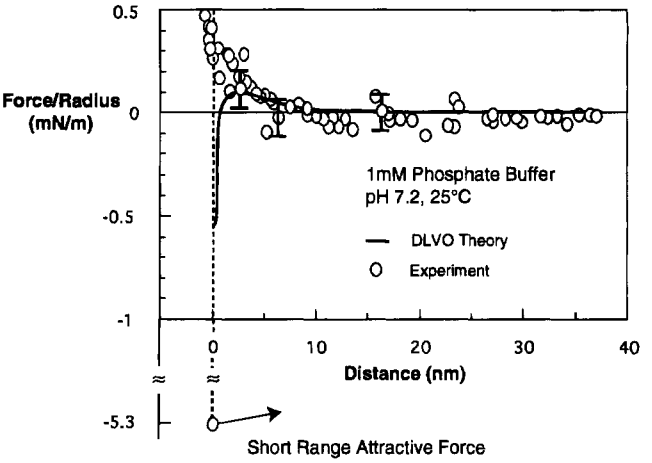

FIGURE 8: Force vs distance profile for the interaction between an oriented 4−4−20 Fab′ monolayer and a 2 mol % DODA-$(EO)_2$-FITC membrane bilayer in 1 mM phosphate buffer at pH 7.2 and 25 °C.

steric forces between reorienting tethered receptor molecules (Leckband et al., 1992, 1994). The fitted Fab′ surface potential was slightly less positive than in the other measurements. This may have been due to a slightly less active preparation. However, when taken together, the average of all Fab′ electrostatic potentials reported in this work was 2 ± 5 mV, and the ±5 mV error is typical of the other data fits described here (*cf.* Figures 2, 3, and 7) and elsewhere (Leckband et al., 1994). Thus, since both the fitted DLVO force and the measured attractive force at $D = 0$ nm were unchanged within experimental error, the specific adhesive force appeared to be unaffected by the fluorescein−lipid dilution. Additionally, the similarities between the values of the specific adhesion measured under conditions that would produce similar cross−bridge densities but dissimilar nonspecific electrostatic forces indicated that the non-DLVO short-range attraction was indeed due to Fab′−fluorescein cross-links and not to nonspecific DLVO forces.

Steric Impediments to Hapten Recognition at Membrane Interfaces. The roughness of the protein surface and the deep Fab′ binding pocket necessitate the incorporation of spacers between the lipid and the hapten in order to optimize hapten accessibility (Ebato et al., 1992, 1994). Although previous studies indicated that 4−4−20 antifluorescyl IgG recognition of fluorescein-presenting monolayers at the air−water interface required only two ethylene oxide units (1.8 nm tether) for hapten recognition (Ebato et al., 1994), an earlier paper suggested that four ethylene oxide units might be optimal (Ebato et al., 1992). In order to determine whether the lower than expected adhesion measured with DODA-$(EO)_2$-FITC was due to an inadequate spacer length, we conducted measurements with DODA-$(EO)_4$-FITC for which the spacer length was 2.3 nm. Although the refractive index of poly(ethylene oxide) is lower than that of water (Arnold et al., 1985), at low DODA-$(EO)_n$-FITC surface densities, the ethylene oxide groups were not expected to alter the local dielectric constant near the surfaces—hence, the van der Waals attraction between the membranes. The group also bears no net charge, and increasing spacer lengths were not expected to affect the long-range electrostatic forces. Thus, the longer tether was only expected to increase the thickness of the fluorescein−lipid monolayer and to possibly enhance the Fab′ adhesion.

As shown in Figure 9, the long-range forces between Fab′ and 5 mol % FITC-$(EO)_4$-DODA were identical to those

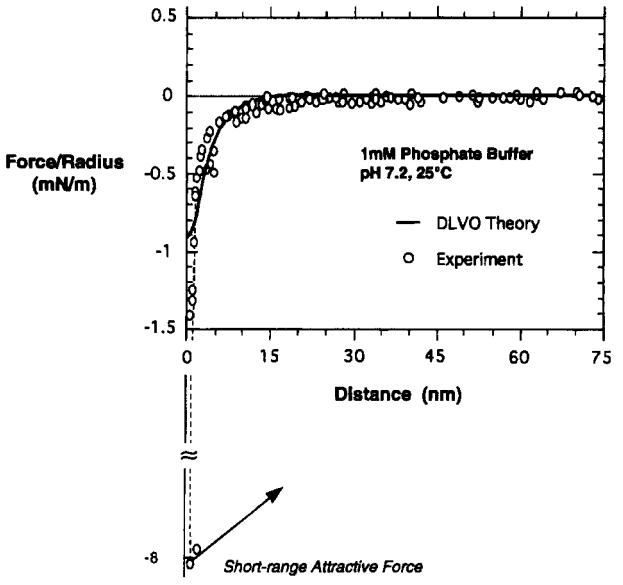

FIGURE 9: Force profile for the interaction between a 4−4−20 Fab′ monolayer and a 5 mol % DODA-$(EO)_4$-FITC membrane bilayer in 1 mM phosphate buffer at pH 7.2 and 25 °C. The open circles represent data from three independent measurements in 1 mM phosphate buffer at pH 7.2 and 25 °C. The solid line is the best fit of the data to DLVO theory, calculated with the parameters given in the text.

measured with FITC-$(EO)_2$-DODA under the same conditions, but the short-range adhesion at $D = 0$ nm increased from −5.0 to −8.1 ± 0.5 mN/m. The apparent total thickness of the fluorescein monolayers increased by 0.4 ± 0.2 nm, as expected, although the surfaces could be easily compressed to the same thickness as measured with DODA-$(EO)_2$-FITC membranes. Analysis of the force curves verified that, within experimental error, the electrostatic surface parameters of both the fluorescein and Fab′ monolayers were unaltered by the increased spacer length; namely, if the outer Helmholtz plane was assumed to lie at the equilibrium separation, then the fitted electrostatic surface potential of the Fab′ monolayer was +7 ± 2 mV (constant potential, Table 1) and the charge density of the 5% fluorescein monolayer was −6 ± 1 mC/m^2 (constant charge density). The magnitude of the specific adhesion increased from −4.7 to −8.0−(−0.9) = −7.1 mN/m. As expected, the increased spacer length had no effect on the long-range forces and therefore only enhanced the magnitude of the short-range adhesive force by increasing the hapten accessibility.

That the long-range forces were unaffected by the tether also directly confirmed the inertness of ethylene oxide to proteins. The efficacy of anchored PEO chains as antiadhesives has been attributed to its ability to create an inert steric barrier against biological adhesion (Jeon et al., 1991). This is attributed to both the chemical inertness of the ethylene oxide monomers to proteins and the repulsive steric barrier effected by large grafted polymer chains. Although the tethers used in these studies are too short to establish the polymeric properties, these measurements directly demonstrate the inertness of the ethylene oxide spacers.

DISCUSSION

These measurements conducted with both active and inactive Fab′ monolayers demonstrated that the forces governing long-range protein interactions are controlled by the composition of the protein exterior. The long-range attractive force law that described the interaction between the Fab′ and negatively charged fluorescein membranes was attributed to the measured positive electrostatic surface potential of the oriented Fab′ monolayer, despite the fact that, at pH 7.2 > $pI_{Fab'}$ (6.8), the protein was negatively charged. Since the homogeneously oriented Fab′ exposed a single surface to the fluorescein membranes, the measured electrostatic potential apparently reflected the composition of the exposed protein surface region rather than of the net protein charge. This was substantiated by comparison of the measured electrostatic properties with both the crystallographically determined 4−4−20 antibody structure (Herron et al., 1994) and the theoretically calculated electrostatic potential contours of the Fab′ fragment (unpublished results). In particular, a ring of positively charged amino acids surrounds the binding pocket of the Fab′ surface (Herron et al., 1994), and the latter charge cluster results in a positive potential surface that completely envelops the binding surface under the ionic conditions used in these measurements (unpublished results).

Changes in the forces effected by the thermal denaturation of the Fab′ conclusively demonstrated that the measured protein electrostatic surface potential and the resultant long-range Fab′−fluorescein force were indeed controlled by the electrostatic properties of the exposed 4-4-20 Fab′ surface. The destruction of the folded Fab′ structure switched the electrostatic double-layer force from attractive to repulsive and abolished the short-range specific adhesion. In contrast to the average electrostatic potential of the native protein (2 ± 5 mV), the effective electrostatic potential of the denatured Fab′ surface was net negative at −55 mV (−2.3 unit charge/Fab′). This was as expected since the denatured protein structure should resemble a random coil polymer with an average surface charge similar to that of the overall protein. Although complete randomization of the structure was unlikely due to the numerous intra- and interchain disulfide bonds that stabilize the Fab′, the structural changes completely altered both the measured Fab′ electrostatic surface properties and the resultant interaction force profiles. Consequently, the forces governing the interactions of Fab′ with membrane-bound haptens clearly depend on the composition of the protein surface as well as on the membrane electrostatics.

The role of the external protein surface in ligand trajectory steering is well-accepted on the basis of theoretical models. Electrostatic surface potential calculations based on continuum theories, for example, predict that topological charge distributions give rise to focusing electrostatic fields that steer ligands into favorable binding orientations (Klapper et al., 1989; Allison et al., 1985; Alison & McCammon, 1985). Previous measurements demonstrated that charged amino acids on the protein surface can give rise to long-range receptor−ligand forces (Leckband et al., 1994). Here, however, we directly demonstrate that the positively charged amino acids near the 4−4−20 Fab′-combining site significantly impact the long-range fluorescein−Fab′ attractive force. This is consistent with previous findings that as few as two amino acids dramatically altered the interaction forces of streptavidin (Leckband et al., 1994). Brownian dynamics simulations and coagulation theory predict that long-range attractive forces would substantially enhance the rates of bimolecular diffusional encounters (Berg & von Hippel, 1985; Luty et al., 1993; Northrup et al., 1987; Koczak &

Subramaniam, 1993). The functional relevance of the streptavidin findings was unclear, but the Fab′−hapten attractive forces measured in this work likely play an important role in molecular recognition. In particular, the near diffusion-controlled 4−4−20 antibody−fluorescein solution binding rate (Krantz et al., 1982; Voss, 1993) is strongly suggestive of electrostatically enhanced binding kinetics. However, since bulk kinetic rates reflect the orientationally averanged bimolecular interaction potentials (Berg & von Hippel, 1985), the average potential governing the fluorescen−4−4−20 Fab′ binding kinetics cannot be directly obtained from these measurements with oriented protein monolayers. However, investigations of the influence of the electrostatic potential fields surrounding monoclonal HyHEL antibodies on the simulated binding to hen egg white lysozyme demonstrated that the protein surface composition near the combining site has the greatest impact on the bimolecular association rates (Koczak & Subramaniam, 1993). Thus, the electrostatic attractive force resulting from the ring of charge near the 4−4−20-combining site most likely plays a similarly important role in the electrostatic guidance of fluorescein docking. These similarities between the HyHEL and 4−4−20 suggest that structure-dependent steering forces may constitute a more general feature of antibody recognition.

These measurements demonstrate good agreement between mean field electrostatic potential calculations and the experimentally determined electrostatic surface properties of the Fab′ surface. Currently, we can only make qualitative statements regarding the comparison between theory and experiment since the surface force measurements report the average electrostatic surface potential over the entire Fab′ monolayer surface. In other words, lateral resolution has been sacrificed for sensitivity. Therefore, neither distinctions between the force contributions of a small inactive Fab′ fraction (~25%) and those of active protein nor the topological variations of individual proteins' electrostatic potential contours are achievable with this method. Although these measurements do not provide the quantitative spatial resolution of theoretical electrostatic potential contours, they do provide *direct* experimental verification of the impact of solvent-accessible charged amino acids on the forces that control protein interactions. Moreover, one directly obtains the distance dependences of these forces and the steric thicknesses of the layers. These measurements support the view that at increased ionic strengths where charges would be less delocalized, differences in local forces due to variations in the protein topology and in the charged amino acid surface map are expected to contribute to more localized steering trajectories that act at distances within ~2 nm of the protein surface.

In this work, the "specific attractive force" was attributed to the non-DLVO contribution to the attractive force at $D =$ 0 nm. Since preferential lipid pull-out rather than specific bond rupture has been observed in a number of other systems with bond energies significantly lower than that of this Fab′−fluorescein pair (Leckband et al., 1995; Bell, 1978; Evans et al., 1992), the short-range non-DLVO adhesive force was tentatively ascribed to the tensile force required to extract fluorescein−lipids from the bilayer (Leckband et al., 1995). Direct evidence for such membrane disruptions was not apparent in these measurements (Leckband et al., 1994, 1995), but the substantial irreversible reduction in the adhesion following successive contacts was consistent with such surface damage and with Fab′ inactivation. In this case, the adhesive force would not directly reflect the intrinsic bond energy, but its magnitude would scale with the numbers of bonds formed (Leckband et al., 1994). Thus, attenuations in the short-range adhesion would reflect changes in the binding probability (Leckband et al., 1994, 1995; Evans et al., 1992; Bell, 1978).

Two possible mechanisms can account for the reduced binding strengths measured with the shorter spacer and at elevated ionic strengths. The steric repulsive forces increased the energy cost of tight fluorescein−anti-fluorescein bond formation, and this may have resulted in a decrease in the number of bonds formed during the time of the measurements. However, this assumes that bond formation was in all-or-none event. The potential for fluorescein and its isomers to partially bind or misbind was demonstrated by the observed differences in the fluorescence lifetimes of bound fluorescein I and II isomers (Swindlehurst & Voss, 1991; Bedzyk et al., 1992). The steric surface forces described in this work could have inhibited full binding site penetration by the fluorescein, which may also have resulted in a reduction in the adhesive strength. Additionally, thermal fluctuations at the interface may enable fluorescein−lipids to undergo transient protrusions and to thereby fully penetrate the binding pocket (Israelachvili & Wennerstrom, 1992). In the latter case, the measured adhesion would reflect a mixed population of fully and partially bound fluorescein. In the absence of additional information, the precise binding perturbations that gave rise to the adhesion attenuation cannot be determined. However, it is clear that the modulation of fluorescein accessibility by surface hydration and by shortening the tether length reduced the probability of tight bond formation—hence, the adhesive strength.

In addition to the electrostatic and van der Waals forces acting between the molecular species, the burying of hydrophobic residues in complexation contributes ~65% to the overall 4−4−20 IgG−fluorescein binding energy (Omelyaneko et al., 1993; Herron et al., 1994). There have been numerous reports of unusually long-range attractive forces extending to separations of up to 90 nm between macroscopic hydrophobic surfaces in aqueous electrolyte solutions (Pashley & Israelachvili, 1982; Pashley et al., 1985; Christenson et al., 1989; Tsao et al., 1993). Although both the 4−4−20 Fab′ binding site and the fluorescein expose substantial hydrophobic surface area, and hydrophobic interactions are clearly essential for tight binding, anomalous long-range forces were not evident in these measurements (*cf.* Figures 4, 5, 7, and 8). These data therefore suggest that the unusual long-range forces between macroscopic hydrophobic surfaces in aqueous solutions do not operate at the molecular level.

By conducting direct force measurements with different hapten spacer lengths and at different ionic strengths, we identified both the molecular origins of forces that control long-range Fab′−hapten interactions and short-range forces and mechanisms that modulate the Fab′ binding to immobilized haptens. In particular, we clearly demonstrated that the interfacial structure can impede site-specific surface binding. The low specific adhesion measured with the 1.8 nm spacer was attributed to interfacial impediments since biotinylated fab′ immobilization to streptavidin monolayers does not result in significant activity losses (Ebato et al., 1992). This was substantiated by the increase in the specific short-range attractive force, but not in the long-range force, attained when the tether length was increased from 1.8 to

2.3 nm. This confirmed that the 1.8 nm tether was too short to accommodate both the geometric requirements of the Fab′ binding site and steric surface barriers (Figure 8). Thus, the spacer length clearly modulated the immobilized hapten accessibility and the consequent binding probability, but it had no effect on the nonspecific forces between the protein and membrane surface.

Previous molecular dynamics studies of antifluorescein monoclonal IgG binding to hapten-functionalized membranes suggested that 1.5 nm would be the minimum spacer length required for the immobilized fluorescein to access the deep antibody binding pocket in the cleft between the V_H and V_L domains (Ahlers et al., 1992). The latter studies did not account for additional interfacial steric barriers such as lipid head group hydration, lipid protrusions, or hydrated ion binding at the membrane surface (Israelachvili, 1992; Pashley, 1982; LeNeveu et al., 1977), all of which would increase the required tether length. Since the measured Stern layer thickness of 5 mol % fluorescein membranes at low ionic strengths was 0.8 ± 0.2 nm per membrane (*cf.* Figure 2), the actual required spacer length would be closer to 2.3 nm, and an increase from 1.8 to 2.3 nm would enhance binding, as observed. Conversely, the 0.8 nm barrier would have reduced the effective length of the 1.8 nm tether to 1.0 nm—less than the minimum length—and thereby reduced the binding probability and, hence, the adhesion. Such binding inhibition by surface hydration may partially explain previous observations that measured Fab′ and IgG binding affinities to DODA-$(EO)_2$-FITC:DPPE monolayers were 40−100-fold lower than those between the soluble species (Ebato et al., 1994; Ahlers et al., 1992). While models based on the molecular dimensions may aid in the accurate predictions of solution binding behavior, these data clearly show that surface binding models must also incorporate the surface properties (e.g. solvation) of the substrate.

It is important to note that although the low adhesion measured with the 1.8 nm spacer was attributed to its short length relative to the steric impediments of both the membrane and protein binding site, the −7.1 mN/m specific attractive force measured with the 2.3 nm tether was still 40% lower than the maximum expected value or −12 mN/m. Part of the discrepancy can be attributed to the ∼15% uncertainty in the protein coverages (Leckband et al., 1995). Fluorescein photobleaching was unlikely since no detectable changes in either the steric thicknesses or the electrostaticproperties of the membranes were observed during measurements between fluorescein−lipid bilayers. However, on the basis of measurements of the membrane hydration thicknesses, the 2.3 nm spacer would barely permit unimpeded access to the immobilized fluorescein. Consequently, steric inhibition is the most likely cause for the low measured values. In particular, the membrane hydration thicknesses could only be measured with an accuracy of ±0.2 nm. As demonstrated in this work, a 0.2 nm difference in the effective spacer length could significantly impact the adhesion. Although this could be easily checked with longer fluorescein spacers, the required fluorescein−lipid conjugates are currently unavailable.

The measurements at increased ionic strengths not only demonstrated the electrostatic origin of the long-range fluorescein−Fab′ attraction but also confirmed the Fab′ sensitivity to the membrane surface properties and the insufficiency of the EO_2 spacer length. Because the solution binding affinity of the 4−4−20 antibody is ionic strength-independent (Herron, unpublished observations), the *ionic strength-dependent* 36% reduction in 4−4−20 Fab′ adhesion measured with the 1.8 nm EO_2 spacer was attributed to changes in the membrane interfacial properties and not to salt-induced changes in the antibody structure or in its intrinsic affinity. In particular, at ionic strengths above the critical hydration concentration, hydrated ions adsorb to hydrophilic surfaces (Pashley, 1982). Although head group solvation would move the membrane steric repulsive force ∼0.3 nm farther out from the lipid head groups, bound hydrated counterions or lipid protrusions could increase the "hydration layer" thickness by up to 3 nm (LeNeveu et al., 1977; Pashley, 1982; Israelachvili & Wennerstrom, 1992). Ionic strength-dependent counterion binding to lipid membrane surfaces has been extensively documented (Pashley, 1982; Marra & Israelachvili, 1985; Leckband et al., 1993; Israelachvili & Pashley, 1982; LeNeveu et al., 1977; McIntosh et al., 1990, 1993). The 1.4 ± 0.2 nm increase in the hydration thickness—0.7 nm/membrane—measured with the 5% DODA-$(EO)_2$-FITC/POPE membranes in 30 mM phosphate buffer at pH 7.2 was consistent with previous measurements with phosphatidylethanolamine mixtures at elevated ionic strengths (Leckband et al., 1993, 1994; Marra & Israelachvili, 1985). At 100 mM Na^+—the counterion in this case—and pH 7.2, the sodium ion concentration exceeded its $> 10^{-2}$ M critical hydration concentration. Thus, the ionic strength-dependent 0.7 nm increase in the Stern layer thickness with the concomitant adhesion attenuation was exactly as expected, particularly if the 1.8 nm spacer was initially too short. Similar salt-dependent reductions in the specific adhesion between streptavidin and biotin lipid-coated surfaces have been measured (Leckband et al., 1994), and the latter phenomenon successfully accounted for slower than predicted rates of site-specific streptavidin adsorption to biotinylated membranes (Balgi et al., 1994).

CONCLUSIONS

These results clearly demonstrated that binding affinities alone do not reflect the complexity of factors that control antibody recognition of tethered receptors. The forces that control both the kinetics and the strength of binding derive from different physical origins and operate at different distances. In particular, we have clearly shown that the protein exterior dictates the magnitude and sign of the long-range forces that likely influence the kinetics of site-specific adsorption. By analogy with other proteins that exhibit similar charge clusters near antigen-combining sites, the molecular basis for the rapid rate of soluble 4−4−20 IgG binding to fluorescein is likely due to the intermolecular attractive electrostatic force attributed to the charge cluster near the 4−4−20 antigen-combining site (Krantz et al., 1982; Voss, 1993). Conversely, the binding probability—adhesion strength—was highly sensitive to the membrane interfacial properties. In particular, membrane solvation and adsorbed solvated ions impeded the Fab′ access to the immobilized hapten and thereby substantially reduced the apparent binding strength. These results imply a remarkable sensitivity to interfacial structure, namely, the ability of Fab′ molecules to detect interfacial perturbations within a few angstroms of the membrane surface. In summary, in addition to the intrinsic receptor−ligand affinities, both the structure of the protein exterior and the membrane interface are important

determinants of the forces that control both the kinetics and strength of specific binding events at membrane surfaces.

REFERENCES

Ahlers, M., Grainger, D. W., Herron, J. N., Lim, K., Ringsdorf, H., & Salesse, C. (1992) *Biophys. J. 63*, 823−838.

Allison, S. A., & McCammon, J. A. (1985) *J. Phys. Chem. 89*, 1072−1077.

Allison, S. A., Ganti, G., & McCammon, J. A. (1985) *Biopolymers 24*, 1323−1336.

Arnold, K., Herrmann, A., Pratsch, L., & Gawrisch, K. (1985) *Biochim. Biophys. Acta 815*, 515−522.

Balakrishnan, K., Mehdi, S. Q., & McConnell, H. M. (1982) *J. Biol. Chem. 257*, 6434−6439.

Balgi, G., Leckband, D., Nitsche, J. M. (1994) *Biophys. J. 68*, 2251−2258.

Bedzyk, W. D., Herron, J. N., Edmundson, A. B., & Voss, E. W. (1990) *J. Biol. Chem. 265*, 133−138.

Bedzyk, W. D., Swindlehurst, C. A., & Voss, E. W., Jr. (1992) *Biochem. Biophys. Act 1119*, 27−34.

Berg, O., & von Hippel, P. H. (1985) *Annu. Rev. Biophys. Biophys. Chem. 14*, 131−160.

Brune, D., & Kim, S. (1994) *Proc. Natl. Acad. Sci. U.S.A. 91*, 2930−2934.

Chan, D., & Horn, R. G. (1986) *J. Chem. Phys. 83*, 5311−5324.

Chan, D., Healy, T. W., & White, L. R. (1976) *J. Chem. Soc., Faraday Trans. 1 72*, 2844−2865.

Christenson, H. K., Claesson, P. M., Berg, J., & Herder, P. C. (1989) *J. Phys. Chem. 93*, 1472−1478.

Ebato, H., Herron, J. N., Müller, W., Okahata, Y., Suci, P., & Ringsdorf, H. (1992) *Angew. Chem., Int. Engl. Ed. 31*, 1087−1090.

Ebato, H., Gentry, C. A., Herron, J. N., Müller, W., Okahata, Y., Ringsdorf, H., & Suci, P. A. (1994) *Anal. Biochem. 66*, 1683−1689.

Evans, E., Berk, D., & Leung, A. (1992) *Biophys. J. 59*, 838−848.

Grabbe, A. (1993) *Langmuir 9*, 797−801.

Häussling, L., Ringsdorf, H., Schmitt, F.-J., & Knoll, W. (1991) *Langmuir 7*, 1837−1840.

Helm, C. A., Laxhuber, M., Lösche, M., & Möhwald, H. (1986) *Colloid Polym. Sci. 264*, 46−55.

Helm, C. A., Knoll, W., & Israelachvili, J. (1991) *Proc. Natl. Acad. Sci. U.S.A. 88*, 8169−8173.

Herron, J. N., Müller, W., Paudler, M., Riegler, H., Ringsdorf, H., & Suci, P. A. (1992) *Langmuir 8*, 1413−1416.

Herron, J. N., He, X.-M., Mason, M. L., Voss, E. W., Jr., Edmundson, A. B. (1989) *Proteins 5*, 271−280.

Herron, J. N., Terry, A. N., Johnston, S., He, X.-M., Guddat, L. W., Voss, E. W., Jr., & Edmundson, A. B. (1994) *Biophys. J. 67*, 2167−2183.

Hunter, R. J. (1989) *Foundations of Colloid Science*; Clarendon Press, Oxford, UK.

Israelachvili, J. (1992) *Intermolecular and Surface Forces*, 2nd ed., Academic Press, New York.

Israelachvili, J. N., & Pashley, R. M. (1982) *Nature 300*, 341−342.

Israelachvili, J., & Wennerström, H. (1992) *J. Phys. Chem. 96*, 520−531.

Jeon, S. I., Lee, J. H., Andrade, J. D., & de Gennes, P. G. (1991) *J. Colloid Interface Sci. 142*, 149−157.

Kibblewhite, J., Drummond, C. J., Grieser, E., & Thistlethwaite, P. J. (1989) *J. Phys. Chem. 93*, 7464−7473.

Klapper, I., Hagstrom, R., Fine, R., Sharp, K., & Honig, B. (1986) *Proteins: Struct. Funct., Genet. 1*, 47−59.

Koppenol, W. H., & Margoliash, E. (1982) *J. Biol. Chem. 257*, 4426−4437.

Kozack, R. E., & Subramaniam, S. (1993) *Protein Sci. 2*, 915−926.

Kranz, D. M., Herron, J. N., & Voss, E. W., Jr. (1982) *J. Biol. Chem. 257*, 6987−6995.

Leckband, D., Schmitt, E. J., Knoll, W., & Israelachvili, J. (1992) *Science 255*, 1419−1421.

Leckband, D., Helm, C. A., & Israelachvili, J. (1993) *Biochemistry 32*, 1127−1140.

Leckband, D., Schmitt, F.-J., Knoll, w., & Israelachvili, J. (1994) *Biochemistry 33*, 4611−4624.

Leckband, D., Müller, W., Schmitt, F. J., Israelachvili, J., & Ringsdorf, H. (1995) *Biophys. J.*, in press.

LeNeveu, D. M., Rand, R. P., Parsegian, V. A., & Gingell, D. (1976) *Nature 259*, 601−603.

Lifschitz, E. M. (1956) *Sov. Phys. JETP (Engl. Transl.) 2*, 73−83.

Luty, B. A., Wade, R. C., Madura, J. D., Davis, M. E., Briggs, J. M., & McCammon, J. A. (1993) *J. Phys. Chem. 97*, 233−237.

Margoliash, E., & Bosshard, H. R. (1983) *Trends Biochem. Sci. 8*, 316−320.

Mara, J. (1986) *Biophys. J. 50*, 815−825.

Marra, J., & Israelachvili, J. (1985) *Biochemistry 24*, 4608−4618.

Marra, J., & Israelachvili, J. (1986) *Methods Enzymol. 127*, 352−360.

Martin, M. M., & Linqvist, L. (1975) *J. Lumin. 10*, 381−390.

Matthew, J. B., Weber, P. C., Salemme, F. R., & Richards, F. M. (1983) *Nature 301*, 169−171.

McConnell, H. M., Watts, T. H., Weis, R. M., & Brian, A. A. (1986) *Biochim. Biophys. Acta 864*, 95−106.

McIntosh, T. J., & Simon, S. A. (1993) *Biochemistry 32*, 8374−8384.

McIntosh, T. J., Magid, A. D., & Simon, S. A. (1990) *Biophys. J. 57*, 1187−1197.

McLaughlin, S. (1989) *Annu. Rev. Biophys. Biophys. Chem. 18*, 113−36.

Müller, W., Ringsdorf, H., Rump, E., Wildburg, G., Spinke, J., Liley, M., & Knoll (1993) *Science 262*, 1706−1708.

Northrup, S. H., Boles, J. O., Reynolds, J. C. L. (1987) *J. Phys. Chem. 91*, 5991−5998.

Northrup, S. H., Boles, J. O., & Reynolds, J. C. L. (1988) *Science 241*, 67−70.

Northrup, S. H., Thomasson, K. A., Miller, C. M., Barker, P. D., Eltis, L. D., Guillemette, J. G., Inglis, S. C., & Mauk, G. A. (1993) *Biochemistry 32*, 6613−6623.

Omelyanenko, V. G., Jiskoot, W., & Herron, J. N. (1993) *Biochemistry 32*, 10423−10429.

Parsegian, V. A., Rand, R. P., & Fuller, N. L. (1991) *J. Phys. Chem. 95*, 4778−4782.

Pashley, R. M. (1982) *Adv. Colloid Interface Sci. 16*, 57−63.

Pashley, R. M., & Israelachvili, J. N. (1991) *J. Colloid Interface Sci. 2*, 169−175.

Pashley, R. M., McGuiggan, P. M., Ninham, B. W., & Evans, E. D. (1985) *Science 229*, 1088−1089.

Sharp, K., Fine, R., & Honig, B. (1987) *Science 236*, 1460−1463.

Sharp, K. A., & Honig, B. (1990a) *Annu. Rev. Biophys. Biophys. Chem. 19*, 301−332.

Sharp, K. A., & Honig, B. (1990b) *J. Phys. Chem. 94*, 7684−7692.

Schmitt, F.-J. & Knoll, W. (1991) *Biophys. J. 60*, 716−720.

Small, D. M. (1967) 4J. *Lipid Res. 8*, 551−555.

Spinke, J., Liley, M.; Schmitt, E. J., Guder, H. J., Angermaier, L., & Knoll, W. (1993) *J. Chem. Phys. 99*, 7012−7019.

Stankowski, S. (1983) *Biochim. Biophys. Acta 735*, 341−351.

Swindlehurst, C. A., & Voss, E. W., Jr. (1991) *Biophys. J. 59*, 619−628.

Tamm, L., & Bartoldus, I. (1988) *Biochemistry 27*, 7453−7458.

Timbs, M. M., Poglitsch, C. L., Pisarchick, M. L., Sumner, M. T., & Thompson, N. L. (1991) *Biochim. Biophys. Acta 1064*, 219−28.

Tsao, Y. H., Evans, E. D., & Wennerström, H. (1993) *262*, 547−550.

Vaknin, D., Kjaer, K., Ringsdorf, H., Blankenburg, R., Piepenstock, M., Diederich, A., & Lösche, M. (1993) *Langmuir 9*, 1171−1174.

Voss, E. W., Jr. (1993) *J. Mol. Recogn. 6*, 51−58.

BI950618Z